# The Belt Pinch - a High-ß Tokamak with Non-Circular Cross-Section

O. Gruber, J.M. Peiry, R. Wilhelm

IPP 1/156 Oktober 1975

**MAX-PLANCK-INSTITUT FÜR PLASMAPHYSIK**

**GARCHING BEI MÜNCHEN**

**MAX-PLANCK-INSTITUT FÜR PLASMAPHYSIK**

**GARCHING BEI MÜNCHEN**

# The Belt Pinch - a High-ß Tokamak with Non-Circular Cross-Section

O. Gruber, J.M. Peiry, R. Wilhelm

IPP 1/156 Oktober 1975

*Die nachstehende Arbeit wurde im Rahmen des Vertrages zwischen dem Max-Planck-Institut für Plasmaphysik und der Europäischen Atomgemeinschaft über die Zusammenarbeit auf dem Gebiete der Plasmaphysik durchgeführt.*

IPP 1/156 O. Gruber, J.M. Peiry, R. Wilhelm

# The Belt Pinch - a High-ß Tokamak with Non-Circular Cross-Section

Abstract

In a Tokamak the attainable ß values are restricted by the limitations of MHD stability. But the necessary improvement of the ß value should be possible by the transition to a non-circular plasma cross-section. In this paper the theoretical conditions for such an improvement are discussed (e.g. volume currents peaked on axis, flattened ends of the elongated cross-section and diamagnetic plasma). Experimental investigations of this problem have been carried out in the Belt Pinch, where plasma production and heating is achieved by fast magnetic compression. This heating method is unusual for a Tokamak, but is for the present the only way to approach the interesting ß-regime ( $\langle ß \rangle \approx 10 - 50\%$) and especially $ß_{pol} > 1$ operation.

As the main result of the Belt Pinch experiments, MHD stability requires about the same $q_{crit}$-value ($\approx 3$) also needed in circular cross-section tokamaks, at least for the present plasma parameters and time scale (b/a ~10, R/a ~7, $\langle ß \rangle \sim 50\%$, $\langle ß_{pol} \rangle \sim 5$, $T_e = T_i \sim 25 - 40$ eV, $\langle n_e \rangle \sim 5 - 7 \cdot 10^{14}$ cm$^{-3}$, values approximately constant for the high-ß-phase of 50 µs). Violating the q-condition, however, fast growing modes destroy the plasma equilibrium within several µs. Compared with such an unstable case, stability for $t \sim 50$ µs means stable behaviour for about 20 MHD growth-times. Numerical calculations indicate a further improvement in present and future experiments with stronger shock-heating and increased temperatures ($T > 100$ eV).

## 1. INTRODUCTION

One of the most serious objections to any tokamak reactor concept with circular cross-section is the limited plasma-ß, which with realistic assumptions ($A \gtrsim 4$, $q_{crit} \gtrsim 3$, $ß_{pol} \lesssim 2$), should be limited to values in the range of only $1 \div 2\%$. One of the best hopes of raising the MHD ß-limit is, on the other hand, the use of non-circular tokamak minor cross-sections /1/. For this reason, some attempt will be made in this direction in several large tokamak experiments in the near future (Doublet, TESEE, Jet). All these experiments, however, use modest b/a-ratios, which, in principle, can only lead to the lower reactor-relevant ß-limit ($\langle ß \rangle \approx 5\%$). It is therefore of interest to follow the way of a non-circular cross-section towards some higher plasma elongations and perhaps some higher ß-values. As pointed out in the theoretical part, special but realistic conditions could allow MHD stability even in the case of such higher b/a-ratios ($b/a > 3 \ldots 4$), in contrast to some previous theoretical work /2/.

If, however, plasma stability comparable with that of the circular cross-section can be obtained under the condition, $q_{crit}$ (elongated) $\approx q_{crit}$ (circular), a large gain in ß for the non-circular cross-section is the result. This is demonstrated in Fig. 1, where possible ß is shown as a function of b/a. The operational regime of the Belt Pinch experiments is also marked in this figure. Starting from a real high-ß equilibrium ($b/a \approx 1o$, $\langle ß \rangle \sim 5o\%$) this regime ends near the classical non-circular tokamak with modest b/a-ratios and the corresponding mean ß-values. At this point it should be added that, in contrast to the classical tokamak, the Belt Pinch uses fast compression for generating and heating the plasma. At least

in the present state of tokamak experiments, only this method yields the two basic requirements for experimental investigation of $\beta_{crit}$ as a function of large b/a:

- the interesting ß-values ( $<\beta> \gtrsim 10\%$) and especially $\beta_{pol} > 1$ can, in fact, be realised experimentally
- no material limiter yields too optimistic stability results.

The stability behaviour of non-circular plasma cross-sections is discussed in the first part of this paper on the basis of present known theory. Then the technical arrangement and the preionization of the Belt Pinch is described. The following section deals with the establishment of the non-circular equilibrium and summarizes the essential plasma parameters and the used diagnostic methods. The stability properties of the Belt Pinch, shown in section 5, leads to a critical q-value. Finally, supporting experiments for the future Belt Pinch programme are presented.

## 2. THEORY

### 2.1 MHD stability: Helical modes ($k \neq o$)

Most theoretical predictions about MHD stability at higher b/a-values are clearly negative /2/. It should be noticed, however, that all these results are obtained under conditions more determined by mathematical simplicity (for instance surface currents) than by optimal but realistic requirements for improved MHD stability. Those requirements, on the other hand, can easily be derived from present known theory. First there is the correct current distribution which can guarantee plasma stability. This is to be seen in the case of circular cross-section in Fig. 2. The stability diagram shown in this figure is based on a toroidal current distribution $j_t = j_o (1-(r/a)^2)^{\nu}$ and a $\beta_{pol} = 1$ /3/. Starting with the homogenous current ($\nu = 0$) or $q_b/q_o = 1$, increasing values of $\nu$ concentrate the current more and more towards the axis. $q_b$ and $q_o$ are the q-values at the plasma surface and on the magnetic axis respectively. Only when $\nu$ becomes larger than two, do stable regions appear with respect to external ($\xi$ surface $\neq 0$) kink modes.

Concentration of the toroidal current, however, means an increasing rotational transform in the centre and possible instability with respect to internal ($\xi_s = 0$) kink modes. The corresponding stability limit in a torus ($q_o \approx 1$) is also marked in the figure. Both limits together allow a reliable operation regime for a tokamak at $q_b \gtrsim 3$ (and perhaps only small windows below) in agreement with experimental observation /1/.

In the case of non-circular cross-section, there are two results, which can be directly compared with Fig. 2. Assuming a pure elliptical cross-section and still $\beta_{pol} = 1$, in the first case, a homogeneous current distribution leads to a still worse stability behaviour /4/. Much more favourable stability behaviour, however, shows the peaked current distribution $j_t \sim \Psi$ ($\Psi$ = poloidal flux function) in the second case /5/. The stability of external modes is equivalent to that of the corresponding circular case with $\nu \sim 2.3$ (Fig. 2) for a fixed q-value. As advantage resulting from improved stability, Fig. 3 shows the critical current densities increasing as a function of b/a /5/. Analysis of this positive result leads to the following conclusion. The unfavourable curvature at the ends of the ellipse is increased by b/a. This negative contribution to plasma stability is compensated by the sum of two effects. Peaked current distribution as well as the fact that the b/a-ratio decreases toward the plasma centre in the case of an elliptic $j_t \sim \Psi$ equilibrium increase the stabilizing shear, i.e. the $q_b/q_o$-ratio. The corresponding decay of $q_o$ (at given $q_b$) may now lead to the problem of internal instability to an extent higher than in the circular case. In addition to the correct current distribution, a second condition should therefore be fulfilled in order to improve non-circular plasma stability. Instead of an ellipse, the non-circular cross-section has to be shaped in race-track-like geometry. Now the advantage of a minimally bad curvature is combined with stretched inner flux surfaces or more or less radially constant b/a-ratio /6/. Owing to the arrangement of the external conductors, the Belt Pinch equilibrium approaches such non-elliptical equilibrium.

The mentioned question of the critical internal $q_o$-value, which must not necessarily be the same as in the circular cross-section, leads to a third requirement in the case of non-circular equilibrium. The discussion of the critical $q_o$ can be based on the necessary Mercier criterion and a new, sufficient criterion derived by Lortz /7/. Both criteria were applied to a toroidal, elliptical equilibrium with a possible admixture of triangulation /8/. As a result, Fig. 4 shows the critical $q_o$-values for the paramagnetic ($\beta_{pol} < 1/2$), the neutral ($\beta_{pol} = 1$) and a diamagnetic ($\beta_{pol} = 2$) case as a function of b/a. From this stability diagram it can be seen that in the case of the present paramagnetic ($\beta_{pol} < 1$) tokamaks the circular, or at most the weakly non-circular, cross-section (with triangulation) has to be preferred for optimal plasma stability. In the case of a diamagnetic plasma, however, the optimum clearly moves to the more non-circular cross-section. It has to be added that the weak diamagnetism of $\beta_{pol} \approx 2$ (now the helix of the field lines and the helix of the plasma current are just equal but counter-rotating) has to be assumed for the future tokamak reactor. Furthermore, the convergence of the necessary and sufficient criterion and the fact that the critical $q_o$ converges to $1/\sqrt{2}$ with increasing b/a is remarkable.

One should mention that, on the other hand, without a conducting wall, a weak diamagnetism has a destabilizing effect with respect to the external kink modes (since the stabilizing internal toroidal field decreases) /9/. A stable behaviour again seems possible if wall stabilization is taken into account /9/ or at very high $\beta_t$-values, since the destabilizing Lorentz forces in the plasma decrease /10/. Considering the toroidal equilibrium limitations, these high $\beta_t$-values can only be achieved at very high half-axis ratios.

The preceding discussion refers to ideal MHD theory (infinite conductivity). Including the effects of resistivity, only a few remarks can be made in the case of non-circular plasma cross-sections. Again a current density peaked on axis helps to stabilize the resistive Tearing modes /4/. Moreover, in case of Tearing modes with very high m-numbers, non-circular plasma cross-sections are less unstable compared with a circular one.

To recapitulate the main results, MHD-stability even at higher b/a-ratios could be expected in case of:

- no surface currents, but peaked volume currents
- no elliptical, but more race-track-like cross-sections
- diamagnetic plasma ($\beta_{pol} > 1$, as assumed in a future tokamak).

Axisymmetric modes (k = 0)

Especially the stronger, non-circular plasma equilibrium seems to be sensitive to displacement instabilities, except for the case of a fully closed outer coil system (flux surface). Besides the stabilizing effect of low aspect ratio ($A < 4$) /11/, cross-sections with flattened ends and volume currents again enhance the stability behaviour compared with elliptical cross-sections and surface current models /12/. The m = 1, k = 0 mode, for example, is unstable for elliptical equilibria with $b/a > 1.4$ ($A \approx 2.5$), whereas more rectangular equilibria become unstable only with $b/a > 4$ ($A \approx 4,5$). Compared with the helical modes, however, the unstable potential of the k = 0-modes is always small /12/. Stability can be achieved by

low-inductance passive multipoles operating like a conducting wall, as has been shown in BP I /13/. Otherwise, the resulting low growth rates allow stabilization by relatively simple feedback methods.

## 2.2 Transport, microinstabilities

In the present Belt Pinch experiments, effects connected with microinstabilities can practically be neglected. In addition, present known theory in any case gives some improvement for the non-circular cross-section compared with the circular one.

Two examples are (fixed $q_b$)

- the Pfirsch-Schlüter effect decreases in proportion to $(a/b)^2$ and independently in the case of high ß-values /14/
- diffusion coefficient of heavy particles towards the plasma centre decreases with increasing b/a /15/.

# 3. APPARATUS

## 3.1 Technical Arrangement

The Belt Pinch experiments up to now have been carried out in three different devices: small Belt Pinch (BP I), large Belt Pinch (BP II / BP IIa) and high-voltage Belt Pinch (HVBP). The essential technical data of these experiments are summarized in Table I. The technical arrangement which is similar in all three experiments, is shown by the example of the BP II apparatus in Fig. 5. The toroidal coil is of rectangular geometry and helically (0.5 turn) wound in its inner part. In this manner, the toroidal field $B_t$ and a fraction of the toroidal plasma current $I_t$ are simultaneously generated. The vertical coil system is installed on the outer surface of the toroidal coil. This system is made of 23 different 2-turn multipoles which operate as a

closed flux surface. In order to obtain the fast programming of the vertical field, necessary for the balance of momentum in the radial direction, the multipole system is connected to the main collector by a variable inductance, parallel to a fast auxiliary vertical field bank. The whole system is energized from a 76o kJ/4o kV bank in conventional technique. The switching system of 128 start and ferrite decoupled Crowbar gaps is installed in 4 sound proof cabinets. Fig. 6 shows a view of the whole arrangement.

The new arrangement for improved shock compression (BP II a) is shown schematically on the left-hand side of the diagram. The horizontal collector now has a bulge corresponding to a small additional inductance of about 1o nH (not existing in the 4o kV experiments). This inductance is enlarged by an effective $\mu \approx 2oo$ of an inner iron core. During the operational time of the pre-magnetized iron from $-\Phi$ to $+\Phi$ (saturation), a fast 12o kV bank is fed in parallel to the enlarged collector inductance, resulting in a peak voltage of 16o kV. The total system has been tested successfully at full voltage /16/.

The discharge chamber, shown in Fig. 7, consists of two coaxial glass cylinders with plane 5 cm thick top and bottom plates. The inner cylinder ( $\phi$ = o.6 m; 2 cm wall thickness) is one piece, whereas the outer tube ( $\phi$ = 1.5m) is made of hard glass plates glued together with epoxy. The basic pressure in the 3.5 $m^3$ volume is typically $< 2 \cdot 1o^{-6}$ torr. Several quartz windows allow optical diagnostics in the UV and IR regions.

## 3.2 Preionization (BP II)

In the shock heated Belt Pinch the preionization has to produce both a highly ionized, radially homogeneous plasma and a low impurity level .Due to the large volume about 1 kJ energy per mTorr $D_2$ filling pressure is needed. The electrical circuit shown in Fig. 8 allows a much lower bank energy (6o kJ, 18 kV) than in a conventional parallel circuit and supplies one half of the bank energy into the toroidal coil. The transmission line filled with iron cores operates like a periodical switch and splits the usually sinusoidal discharge into discrete pulses as is shown in Fig. 8. Depending on the flux which can be absorbed by the iron cores (0.5 Vs) everytimes at the beginning and at the end of the first, third ... current pulse the transmission line is blocked for the high voltage of the main discharge for a sufficiently long time.

The ignition of the preionization is done by a capacitively coupled high-frequency generator producing a weakly ionized plasma with an electron density of about $1o^{11}$ $cm^{-3}$. In the following preionization discharge the plasma is further ionized by the toroidal and poloidal plasma currents. The first current pulse gives a tokamak like discharge with a homogeneous low ionized plasma at the end of the current pulse. At the beginning of the following current pulses a break-down and a magnetic compression occur . The plasma column could be kept in a good toroidal equilibrium and was homogeneous at the beginning of the next current pulse (see end-on smear picture in Fig. 8).

The ionization degree was determined by measuring the area electron density with an Ashby interferometer (3.4 μm) and taking the plasma dimensions from the optical observations. At the end of the first current pulse the ionization degree reaches values of 1o% (5 mTorr $D_2$ filling pressure) and 4o% (2 mTorr $D_2$) and increases to $\geq$ 5o% after the second current pulse. These values agree with further estimates using the absorbed plasma energy from the preionization bank and the calculated line mass from the bouncing frequency. As previous experiments /13/ have shown the impurity level increases with the number of the preionization pulses, therefore the main bank was fired just before the third pulse. Under these conditions the main discharge led to a high-ß plasma and the measured oxygen content is lower than o.4% at a filling density of 5 mTorr $D_2$.

## 4. EXPERIMENTS

### 4.1 Plasma equilibrium

The non-circular plasma equilibrium needs the shaping forces of a conducting wall or coil system. The basic question concerning the permissible wall distance was answered by experiment /13/ and theory /6, 17/ with the following result. The radial plasma compression ratio $\kappa = A/a$ has to be about two or at most three in order to obtain half-axis ratios $b/a > 2$. This entails a serious problem in the case of a compressionally heated plasma since shock heating already yields to a plasma compression of up to 4. Energy losses (radiation, ionization) would still increase the compression ratio. As a consequence, the shock-heated and adiabatically compressed plasma is overcompressed and contracts axially until its final equilibrium state with $\kappa \approx 3$ is reached.

In the experiments, a strong axial contraction results in unstable plasma behaviour which is shown in the end-on smear picture of Fig. 9. Therefore this axial contraction has to be avoided carefully, which can be done in three ways: reduction of adiabatic plasma heating, strong field diffusion and slow axial contraction controlled by external multipole currents.

In the first Belt Pinch experiments (BP I), the small dimensions and fast temperature decay due to impurity line radiation led to fast plasma diffusion and correspondingly to a weakly compressed equilibrium state /13/. The new, larger experiment (BP II) was constructed to improve the plasma confinement at higher temperatures and plasma ß. In this situation of only small field diffusion, a non-circular high-ß equilibrium could be obtained with practically no adiabatic heating and small axial contraction. Consequently, operation was at a toroidal field of 0.15 T with practically constant amplitude for 1 msec. The resulting time behaviour of the toroidal magnetic field and the toroidal plasma current is shown in Fig. 1o.

## 4.2 Plasma parameters (BP II)

For statements on the stability behaviour of the non-circular cross-section, the basic plasma parameters have to be known. These parameters, viz. plasma-ß, temperature, density, magnetic fields, and plasma geometry, were determined using the conventional diagnostic methods. The mean toroidal ß-value

$$\langle \beta_t \rangle = 1 - \frac{\langle B_{ti}^2 \rangle}{B_{te}^2} \approx \frac{\langle p \rangle}{B_{te}^2/8\pi}$$

($B_{te,i}$ = external (internal) toroidal magnetic field)

was evaluated in two different ways. Besides the well-known diamagnetic probe techniques,

in the case of $\beta_{pol} > 1$ - operation, the toroidal pressure balance also gives the required $\beta_t$-information according to

$$B^2_{pol}\,(+A) - B^2_{pol}\,(-A) = 4\,\frac{a}{R}\,\langle\beta_t\rangle\quad B^2_{te} + 0\,\left(\frac{a^2}{R^2}\right)$$

($B_{pol}\,(\pm A)$ = poloidal field at outer (inner) boundary).

In the high-ß-equilibrium of Belt Pinch II, the two independent measurements were in good agreement. The resulting total $\beta_{tot}$ is shown in Fig. 7 as a function of time. During this relatively long period with high toroidal ß, the poloidal ß-value

$$\langle\beta_{pol}\rangle = \frac{\langle p\rangle}{\overline{B_{pol}}^2/8\pi} = 1 + \langle\beta_t\rangle\,\frac{B^2_{te}}{\overline{B_{pol}}^2}$$

($\overline{B_{pol}}$ averaged over the poloidal circumference)

comes close to its theoretical maximum at $\langle\beta_{pol}\rangle \approx A$ ($\approx 7$ in BP II).

The time behaviour of $\langle\beta_{pol}\rangle$ is also shown in Fig. 10. After 70 µs the plasma is confined by the poloidal magnetic field only ($\beta_{pol} \sim 1$; $\beta_t = 0$).

Direct probe measurements inside the plasma are only possible in the early stage of the discharge. The radial profiles of the two field components and the evaluated pressure profile is shown in Fig. 11 at a time before the final axial equilibrium state is reached ($\chi > 3$). As indicated by the radial profile of the poloidal field, the induced toroidal plasma current is already concentrated in the plasma core at this early time (t = 15 µs). The position of the separatrix, also marked in the figure, is estimated according to the flux which is fed into the system by the external vertical coils. The large difference between $B_{pol}$ at the outer and inner plasma surface, finally, is significant for the operation at the mentioned high poloidal ß-value.

The plasma density was determined by Ashby interferometry giving together with the measured axial plasma dimension a peak electron density of $1o^{15}$ $cm^{-3}$ at the end of the heating phase (5 mTorr filling density). The electron temperature in the centre of the plasma was measured by Thomson scattering. The high stray light level (glass vessel without special window) was reduced by using a polychromator and individual interference filters in different channels. Fig. 12 shows the time dependence of the electron temperature, which decreases in accordance with the $\beta_{tot}$ measurements after the main field is crowbarred.

The plasma parameters obtained for the standard conditions of 5 mTorr $D_2$ filling pressure are given in Table II. The energy confinement $\tau_E \approx 35\,\mu s$ is estimated including the plasma heating by the diffusing toroidal field and the toroidal plasma current and was limited by impurity radiation. The strong influence of this loss mechanism was demonstrated by adding a fraction of oxygen comparable with the natural oxygen content of the discharge. In this case, the ß-decay was increased as expected.

A first improvement of the high-ß time scale was obtained by using a lower filling pressure (2 mTorr $D_2$). At practically constant impurity level, the influence of the radiation was reduced and the ohmic heating becomes more effective. The measurements indicated a correspondingly slower decay of the plasma diamagnetism.

A further improvement of the confinement times is expected from using the new fast high-voltage system described in 3.1 (BP IIa). A temperature range above 1oo eV should then be obtainable after thermalization and the lower ionization stages of the impurities are burnt out, which reduces the radiation losses by nearly an order of magnitude. According to a numerical diffusion code, that includes several energy loss mechanisms, i.e. impurity radiation, heat conduction and effects of neutrals, an energy confinement time of o.5 ms should be achievable /18/.

## 5. STABILITY BEHAVIOUR

The MHD stability as the crucial point of the non-circular plasma cross-section has been investigated in more detail and under different boundary conditions. In all experiments and at different values of ß, $ß_{pol}$, and b/a, the q-limit for stability was found to be of the same order as in a circular tokamak. Below the common critical q-value of around 2 - 3 (at the boundary), the plasma behaves in a highly unstable manner. Operating in this unstable regime, a distinction could be made between three different types of modes observed in BP I with the help of the transparent coil system /13/:

- Very high m-modes ("filaments") at $q_b > 3$ (or even higher) and $ß_{pol} > 1$. Such instabilities were only observed during the very early stages of the discharge in BP I (see Fig. 14a) . It can be assumed that these modes are caused by the surface currents and become stable when the toroidal current becomes peaked on the axis during the discharge ($q_b / q_o > 2$; see also Fig. 2).
- Higher m and n modes (typically m = 4, n = 2 - 3 ) at $q_b \approx 1 - 2$ and $ß_{pol} \approx 1$. An example is shown in Fig. 14b.
- m = 1-like modes at $q_b < 2$ and $ß_{pol} \approx 1$ (see Fig. 14c).

In most cases the m = 1-like modes develop from a higher m-mode coming earlier in time.

All these modes are growing in a time scale of typically several microseconds. Now increasing the q to values around or above three, the plasma behaves in a stable manner at least for the limited experimental time scale. The improvement of plasma stability by only a small variation in $q_b$ is shown in Fig. 15 for the high-ß equilibrium of BP II (plasma parameters are given in Table II). The two streak pictures in this figure (view of

minor cross-section 2a) are obtained under exactly the same plasma conditions (temperature, ß, toroidal field, toroidal plasma current). The only difference between the stable case A and the unstable case B is a weakly decreased b/a-ratio in the case B, programmed by the external multipole system. The corresponding time dependence of the q-values at the plasma surface defined by

$$q_b = \oint \frac{B_t}{B_{pol}\, 2\pi\, R}\, d\,\ell_{pol}$$

is also shown in the figure. The instability (B) develops after 25 $\mu$s when the $q_b$-value falls below 3.

A more precise statement about this obvious stability limit can be obtained by comparing the stable period $\tau_s$ of the high-ß equilibrium with the growth time $\tau_i = 1/\omega_i$ of the instabilities in case B. The result

$$\omega_i\, \tau_s \approx 20$$

means improved plasma stability for about 20 MHD growth times by only a small q-variation of about 20% from above to below the stability limit. In addition, it should be pointed out that the observed growth rate $\omega_i \approx 3 \cdot 10^5\ s^{-1}$ agrees with the characteristic MHD growth rate

$$\omega_{MHD} = \overline{B_{pol}} \,/\, \sqrt{4\pi\rho a^2} \qquad (\rho = \text{mass density}).$$

One should also mention that the three favourable conditions claimed by the theory (see Section 2) are realised in the BP II experiment. The stabilizing effect of a finite Larmorradius may also exist at least for higher m-modes ($a/r_{L,\ ion} \approx 10$).

## 6. SUPPORTING EXPERIMENTS (HVBP, BP IIb studies)

The Belt Pinch experiments may give a physical basis for a future tokamak approach to stronger non-circular equilibria. For this purpose, however, a further improvement of temperature and confinement time towards present-day tokamak standard has to be considered.

The physical and technical preparation has already been started in two supporting experiments. The physical problems concerned with the very rapid shock compression at electrical fields of 1 kV/cm are studied in the high-voltage Belt Pinch (HVBP). In first experiments, a weakly compressed plasma has been produced with densities of $1 - 2 \cdot 10^{14}$ cm$^{-3}$. Neutron flux measurements indicate an ion energy of 1.5 keV. Electron temperatures in the keV region have also been observed in the current-carrying region of the pressure gradient by laser scattering /19/. Ion relaxation, final plasma-ß, resistivity and diffusion now will be studied within the given limited plasma lifetime.

The technical problems in combining compression with MV voltages and the required millisecond pulse time has been solved with a new concept for fast pulsed magnetic fields. In a model experiment corresponding to a disc of 1/25 the height of the future BP IIb, a fast-rising ($\tau \approx 1$ µs) current of 1 MA could be maintained for several ms /20/.

## 7. CONCLUSIONS

In the Belt Pinch, the strong shock heating allows to investigate the advantage of the non-circular plasma cross-section at the relevant high-ß and $ß_{pol}$ values. Up to now, it has been shown that non-circular cross-sections with much higher half-axis ratios than the commonly assumed optimum at $b/a \approx 2$, can be stable at $q_b \gtrsim 3$. At present, this experimental statement is restricted to the typical MHD gross modes and refers to a highly diamagnetic plasma ($ß_{pol} \approx A$) with a peaked current distribution and presumably a plasma cross-section with flattened ends and stretched inner surfaces. In particular, it should be pointed out that the necessary q-value is comparable with that of the circular cross-section in a low-ß tokamak.

Finally, we note besides the higher possible ß-values the additional advantage of a large half-axis ratio, that for high toroidal plasma currents only low toroidal magnetic fields are necessary ($I_t \approx 100$ kA, $B_t \approx 0.15$ T in the experiment).

Acknowledgement

The authors wish to thank H. Röhr for the laser scattering measurements and H. Krause for valuable discussions.

TABLE I

Experimental parameters of the Garching Belt Pinches

| | BP I | BP II | BP IIa | HVBP |
|---|---|---|---|---|
| 2 B [cm] | 1o4 | 26o | | 118 |
| 2 A [cm] | 17 | 45 | | 24 |
| $R_t$ [cm] | 23 | 53 | | 3o |
| U [kV] | 4o | 4o | 16o | 25o |
| E [V/cm] | 16o | 65 | 26o | 7oo |
| $B_t$ ($R_t$) [T] | o,8 | o,6 | | o,3 |
| $I_t$ [kA] | 1oo .. (4oo) | 1oo .. (5oo) | | 2oo .. 3oo |
| $\tau$ pulse* [µs] | 3oo | 1ooo | | 1 / 5o** |

* decay to 8o% of $B_{max}$

** with prepared crowbar system

TABLE II

Measured plasma parameters in the BP II - experiment

$\langle n_e \rangle \sim 5 \cdot 10^{14}$ cm$^{-3}$

$\langle T_e \rangle \sim 25$ eV

$b/a \sim 10 - 14$

$R/a \sim 7$

$\langle \beta_{tot} \rangle \sim 0.5$

$\langle \beta_{pol} \rangle \sim 5$

} for the high-ß phase

$I_t \sim 200$ kA

$B_t \sim 0.15$ T

} decay $\gtrsim$ 1 ms

oxygen content $\sim 0.4$ %

$\tau_E \sim 30 - 40$ µs

References

/1/ H.P. Furth, Nucl. Fusion 15, 487 (1975)

/2/ J.B. Freidberg, F.A. Haas, Phys, Fluids 17, 44o (1974)
B. Marder, Phys. Fluids 17, 447 and 634 (1974)

/3/ J.A. Wesson, A. Sykes, Tokyo Conf. 1974, IAEA - CN - 33/A 12-3

/4/ G. Laval, R. Pellat, J.S. Soule, Phys. Fluids 17, 835 (1974)

/5/ G. Laval, R. Pellat, 6th European Conf. on Contr. Fusion and Plasma Phys., Moscow (1973) Vol. II, p. 64

/6/ F. Herrnegger, E.K. Maschke, Nucl. Fusion 14, 119 (1974)

/7/ D. Lortz, Nucl. Fusion 13, (1973)

/8/ D. Lortz, J. Nührenberg, Nucl. Fusion 13 (1973)

/9/ J.B. Freidberg, J.P. Goedbloed, 3rd Top. Conf. on Pulsed High-Beta Plasmas, Culham (1975)

/1o/ O. Gruber, IPP-Report 1/152 (1975), Garching

/11/ E. Rebhan, A. Salat, 7th European Conf. on Contr. Fusion and Plasma Phys., Lausanne (1975), Vol. I, p. 1o1

/12/ M. Okabayashi, G. Sheffield, Nucl. Fusion 14, 263 (1974)
M.D. Rosen, MATT-Report 1o63 (1974)

/13/ H. Krause, IPP-Report 1/15o (1974) (to appear in Nucl. Fusion)

/14/ J. Nührenberg, Nucl. Fusion 12, 383 (1972)

/15/ T. Ohkawa, Gen. Atomic Comp., Report GA-A 12016 (1974)

/16/ O. Gruber, R. Wilhelm, 7th Europ. Conf. on Contr. Fusion and Plasma Physics, Lausanne (1975), Vol. I, p. 43

/17/ G. Becker, Nuc. Fusion 14, 319 (1974)

/18/ G. Becker, D. Düchs, 3rd Top. Conf. on Pulsed High-Beta Plasmas, Culham (1975)

/19/ F. Soeldner, K.H. Steuer, 3rd Top. Conf. on Pulsed High-Beta Plasmas, Culham (1975)

/20/ R. Wilhelm, 3rd Top. Conf. on Pulsed High-Beta Plasmas, Culham (1975)

FIGURE CAPTIONS

Fig. 1 Possible gain in ß as a function of b/a

Fig. 2 Stability diagram for different current distributions (circular cross section, $ß_{pol} = 1$) without a conducting wall

Fig. 3 Critical current density as a function of b/a ( $j_t \sim \Psi$ , $ß_{pol} = 1$, external kink modes)

Fig. 4 Critical $q_o$ - values as a function of b/a

Fig. 5 Technical arrangement of the BP II - experiment

Fig. 6 View of the Belt Pinch II arrangement

Fig. 7 View of the glass vessel in Belt Pinch II

Fig. 8 Preionization of the BP II - experiment: streak picture (minor cross section), toroidal plasma current and toroidal field

Fig. 9 Streak pictures of an adiabatically compressed plasma (BP II: $B_t = 4$ kG, $I_t = 325$ kA). View of minor cross section (top) and side-on (bottom).

Fig. 1o Time behaviour of $I_t$ , $B_t$, $ß_{pol}$ and $ß_{tot}$ for the standard case in BP II (5 mTorr $D_2$, 4o kV)

Fig. 11 Radial profiles of the magnetic fields (bottom) and resulting pressure profile (BP II)

Fig. 12 Axial profiles of the poloidal field at the outer coil surface (BP II)

Fig. 13 Time behaviour of electron temperature in the plasma centre (main field crowbarred at 9 us)

Fig. 14 Different unstable modes (BP I - experiment)

a) "filaments", high-m modes

b) $m = 4$, $n = 3$ mode at $q_b \sim 1.5$

c) $m = 1$, $n = 1$ mode at $q_b \sim 1 \div 2$

Fig. 15 Streak pictures (minor cross section) at stable (A) and unstable (B) conditions (BP II)

Time behaviour of the corresponding $q_b$ - values

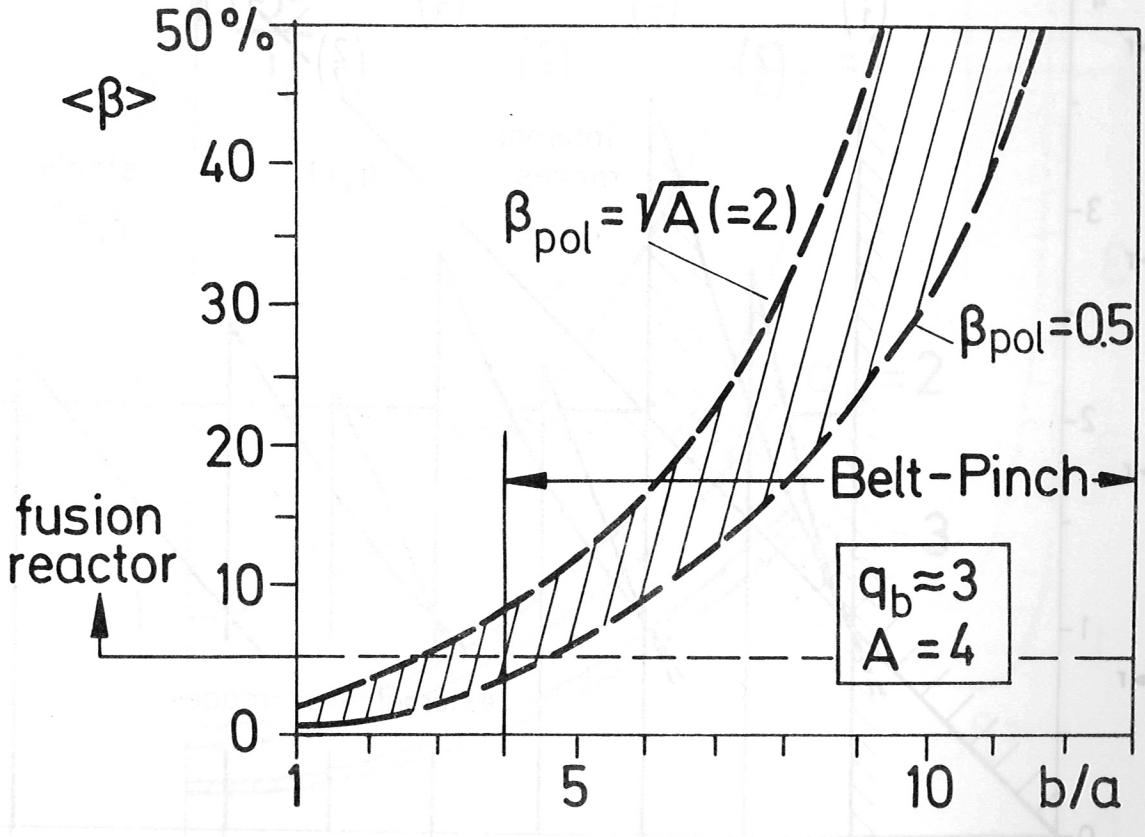
50 %
<β>
40
30
20
10
0
fusion
reactor
$\beta_{pol} = \sqrt{A}\,(=2)$
$\beta_{pol}=0.5$
Belt-Pinch
$q_b \approx 3$
$A = 4$
1
5
10
b/a

Fig. 1

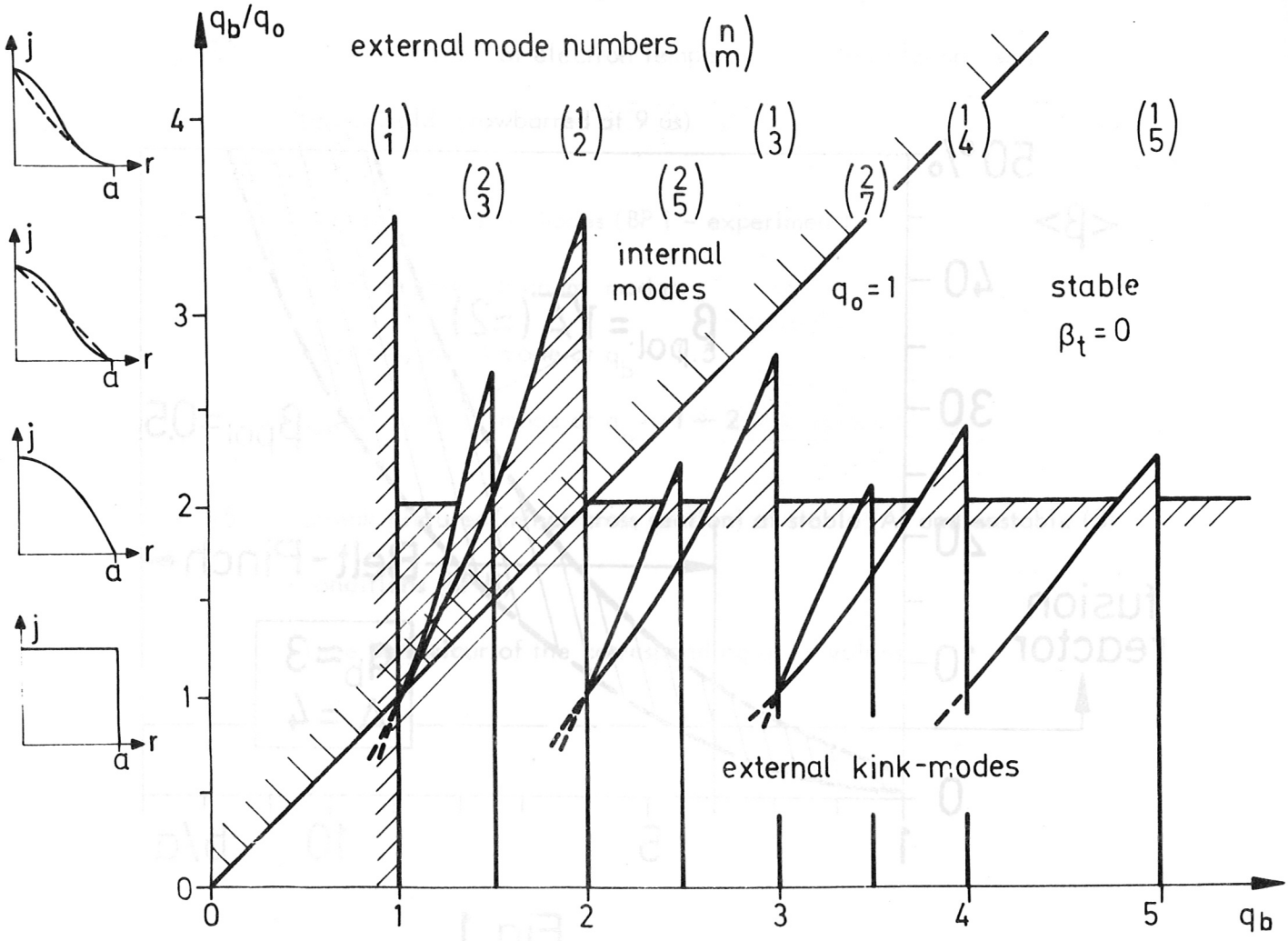
$q_b/q_o$
external mode numbers $\binom{n}{m}$
$\binom{1}{1}$
$\binom{2}{3}$
$\binom{1}{2}$
$\binom{2}{5}$
$\binom{1}{3}$
$\binom{2}{7}$
$\binom{1}{4}$
$\binom{1}{5}$
internal modes
$q_o = 1$
stable
$\beta_t = 0$
external kink-modes
j
r
a
0
1
2
3
4
5
$q_b$

Fig. 2

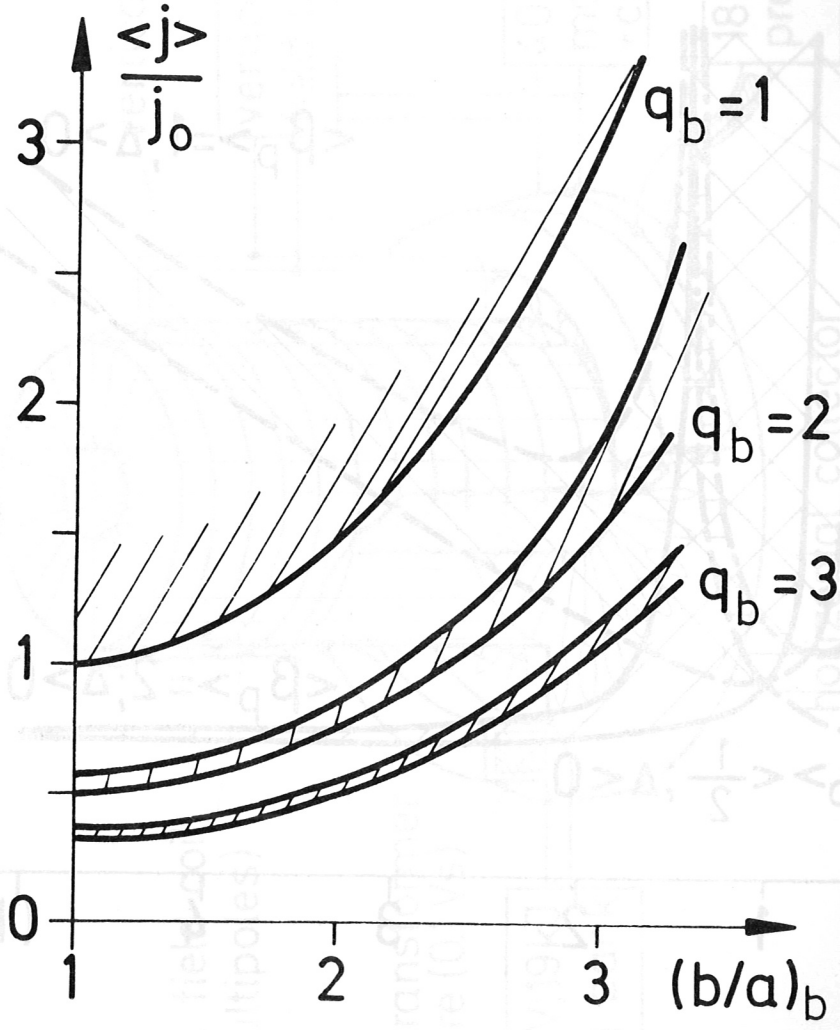


Fig.3

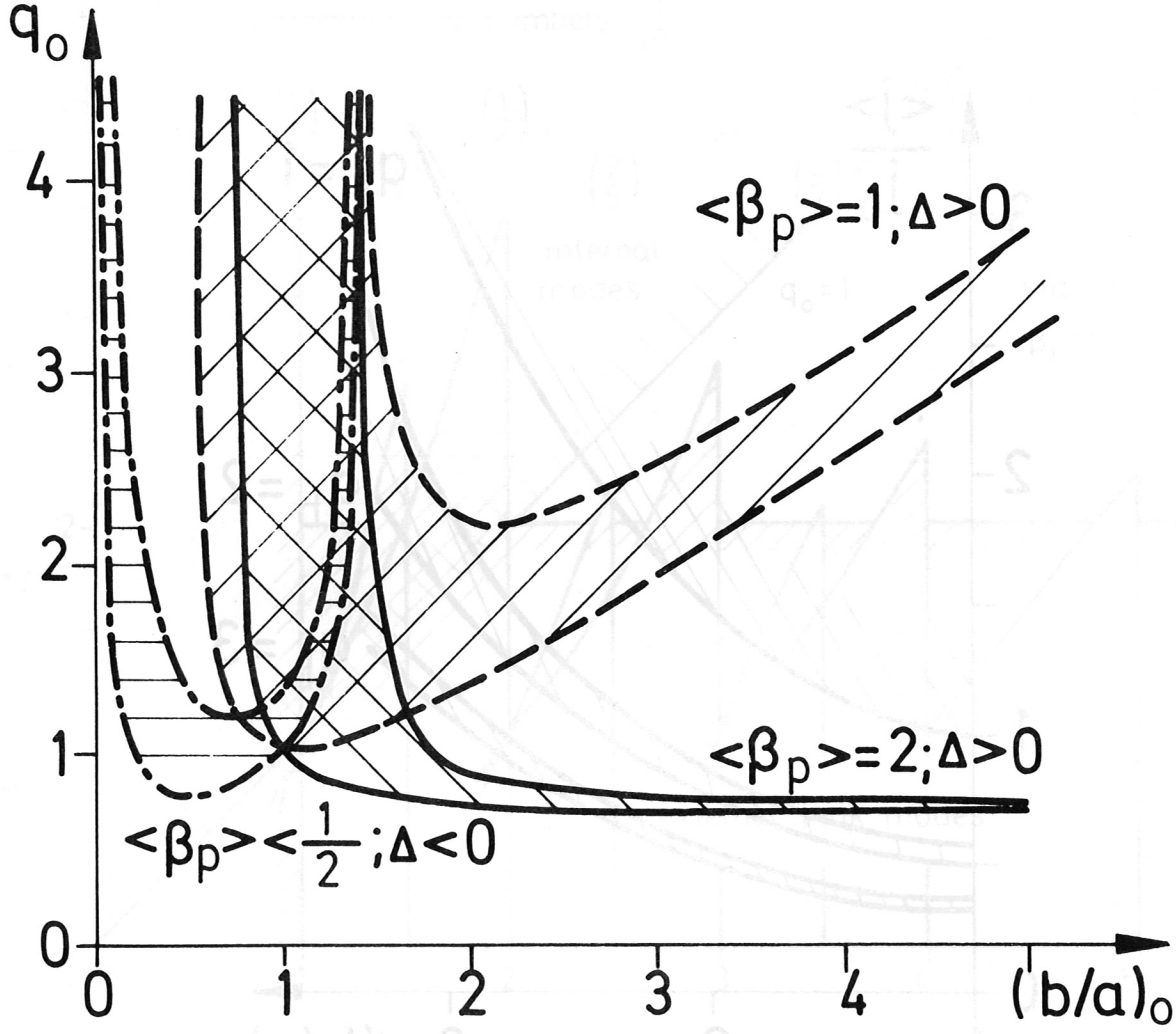
$q_o$
4
3
2
1
0
0
1
2
3
4
$(b/a)_o$
$<\beta_p>=1;\Delta>0$
$<\beta_p>=2;\Delta>0$
$<\beta_p><\frac{1}{2};\Delta<0$

Fig. 4

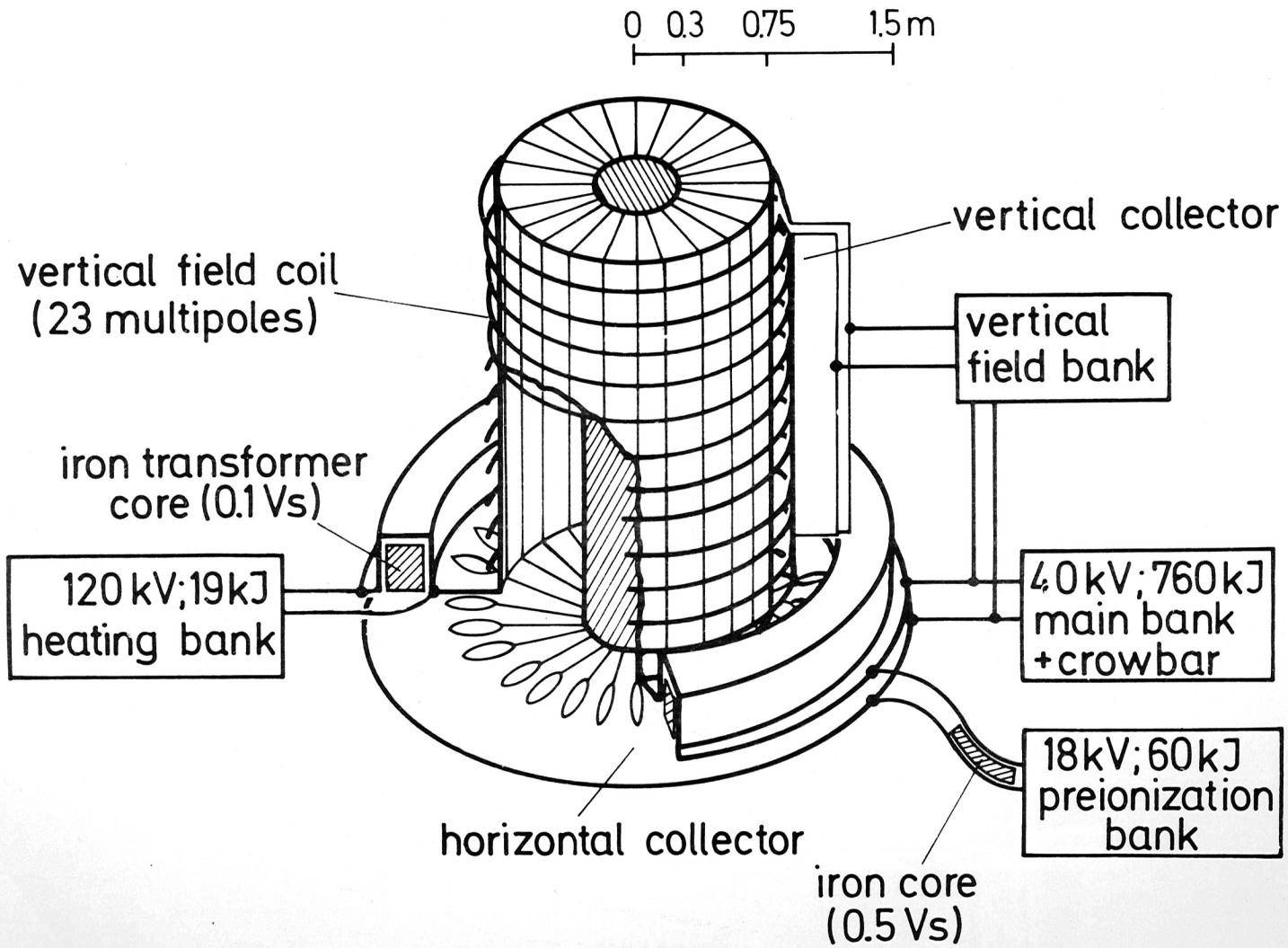
0 0.3 0.75 1.5 m
vertical collector
vertical field coil
(23 multipoles)
vertical
field bank
iron transformer
core (0.1 Vs)
120 kV; 19 kJ
heating bank
40 kV; 760 kJ
main bank
+ crowbar
18 kV; 60 kJ
preionization
bank
horizontal collector
iron core
(0.5 Vs)

Fig. 5

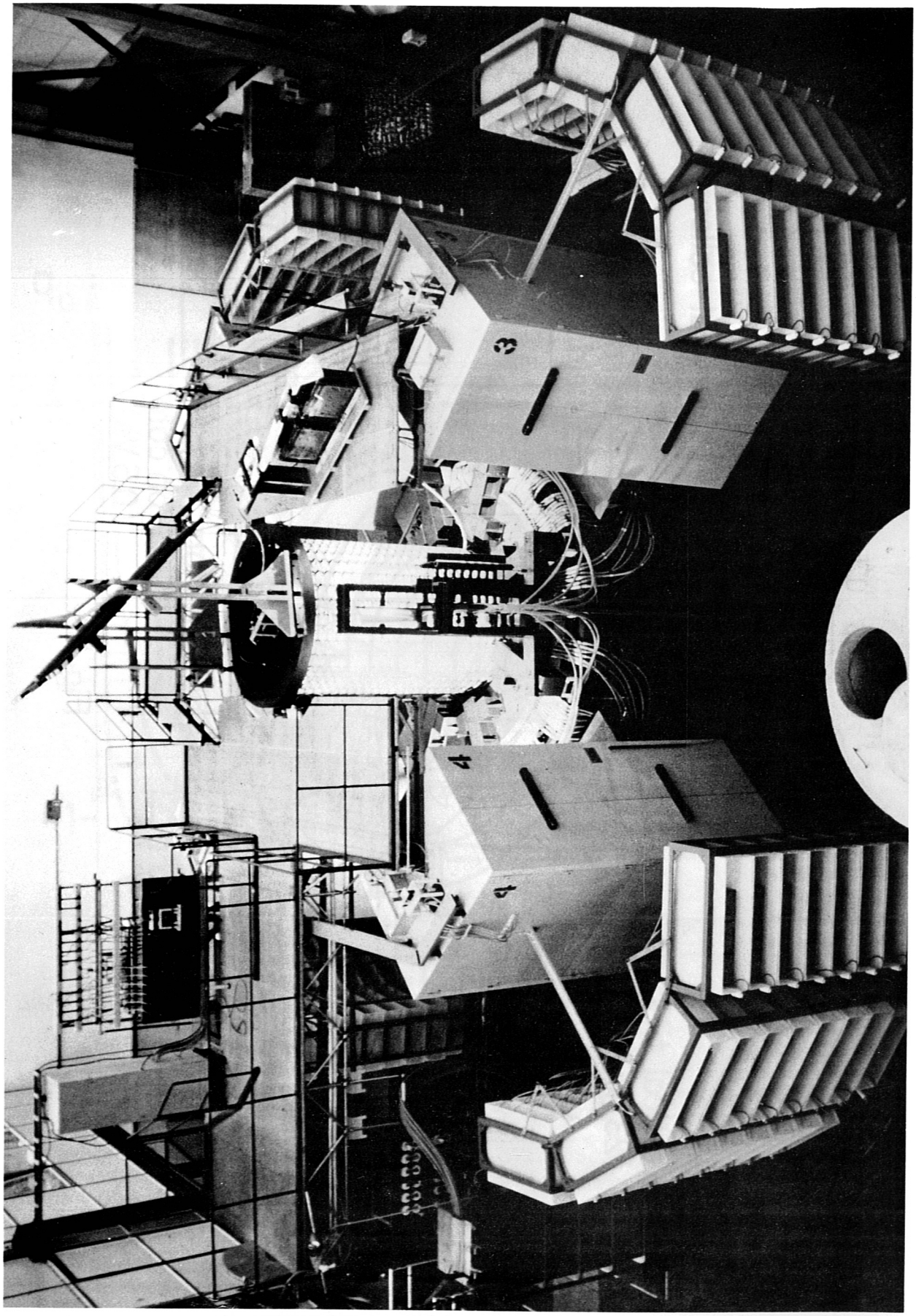

Fig.6

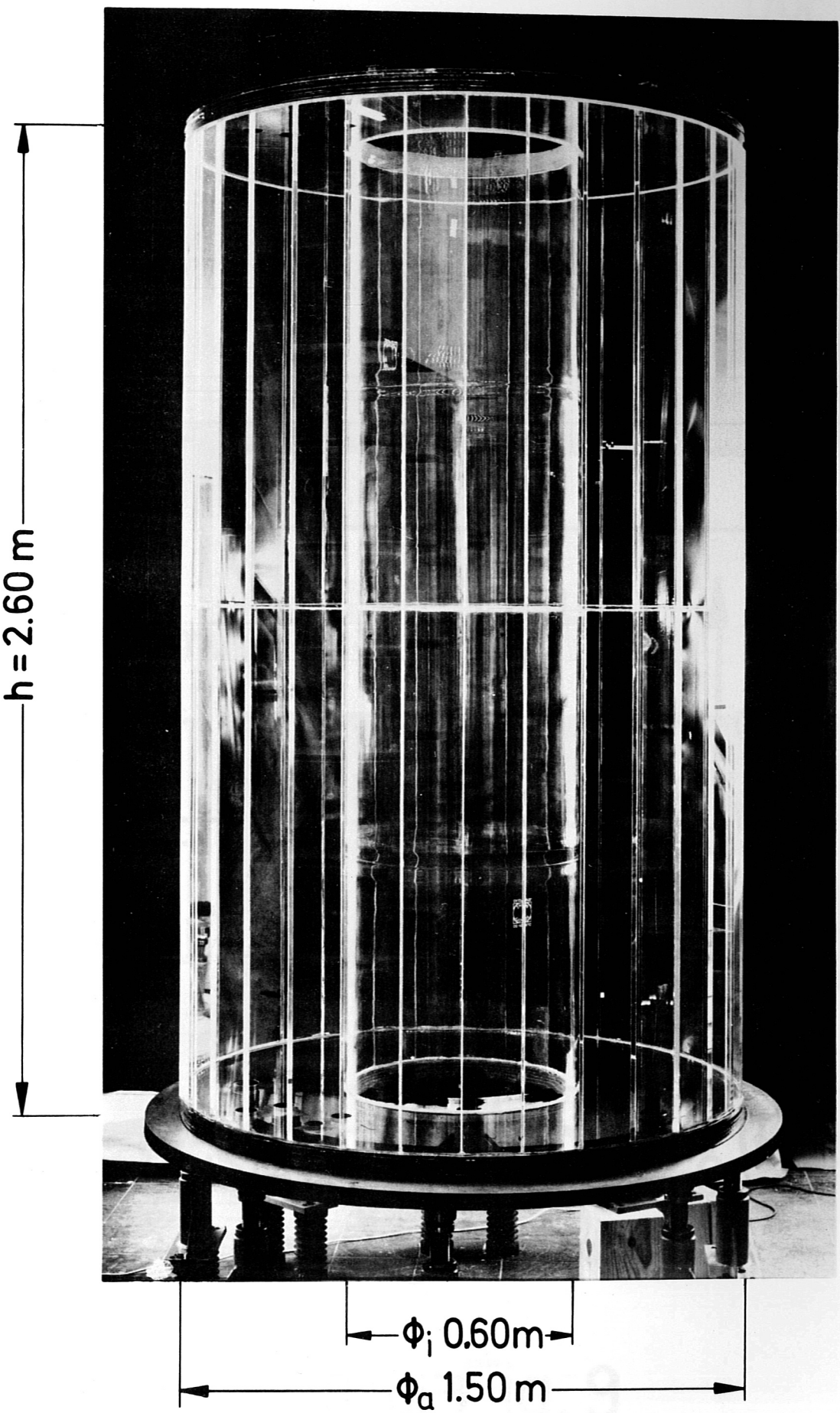


Fig.7

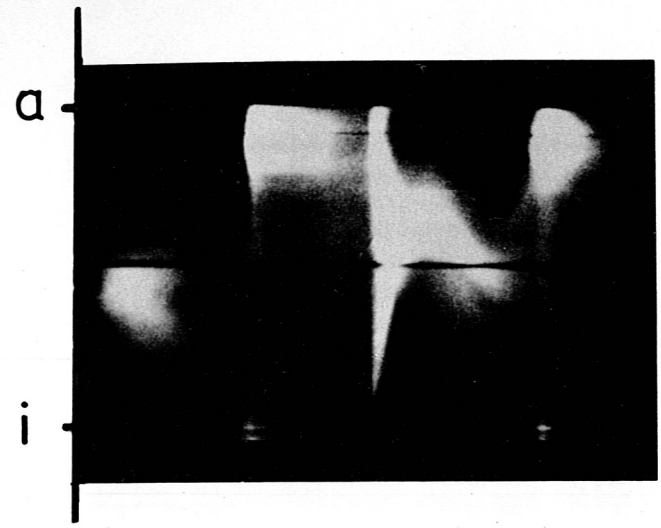


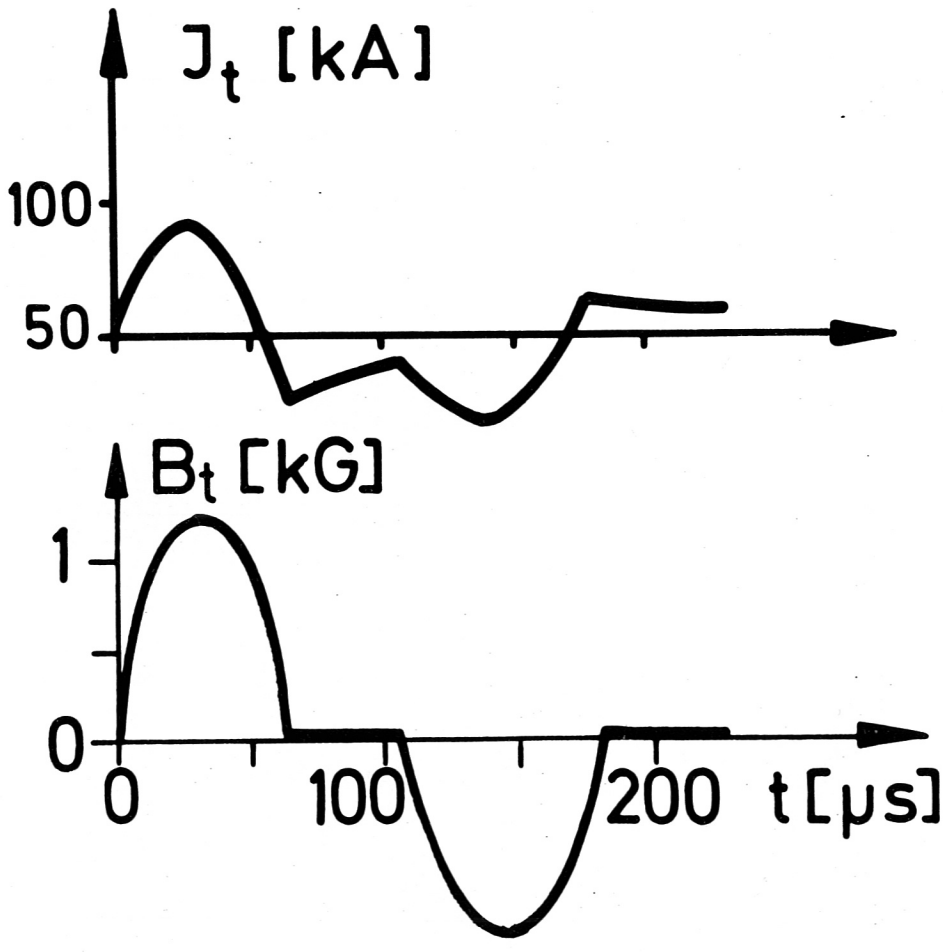


Fig. 8

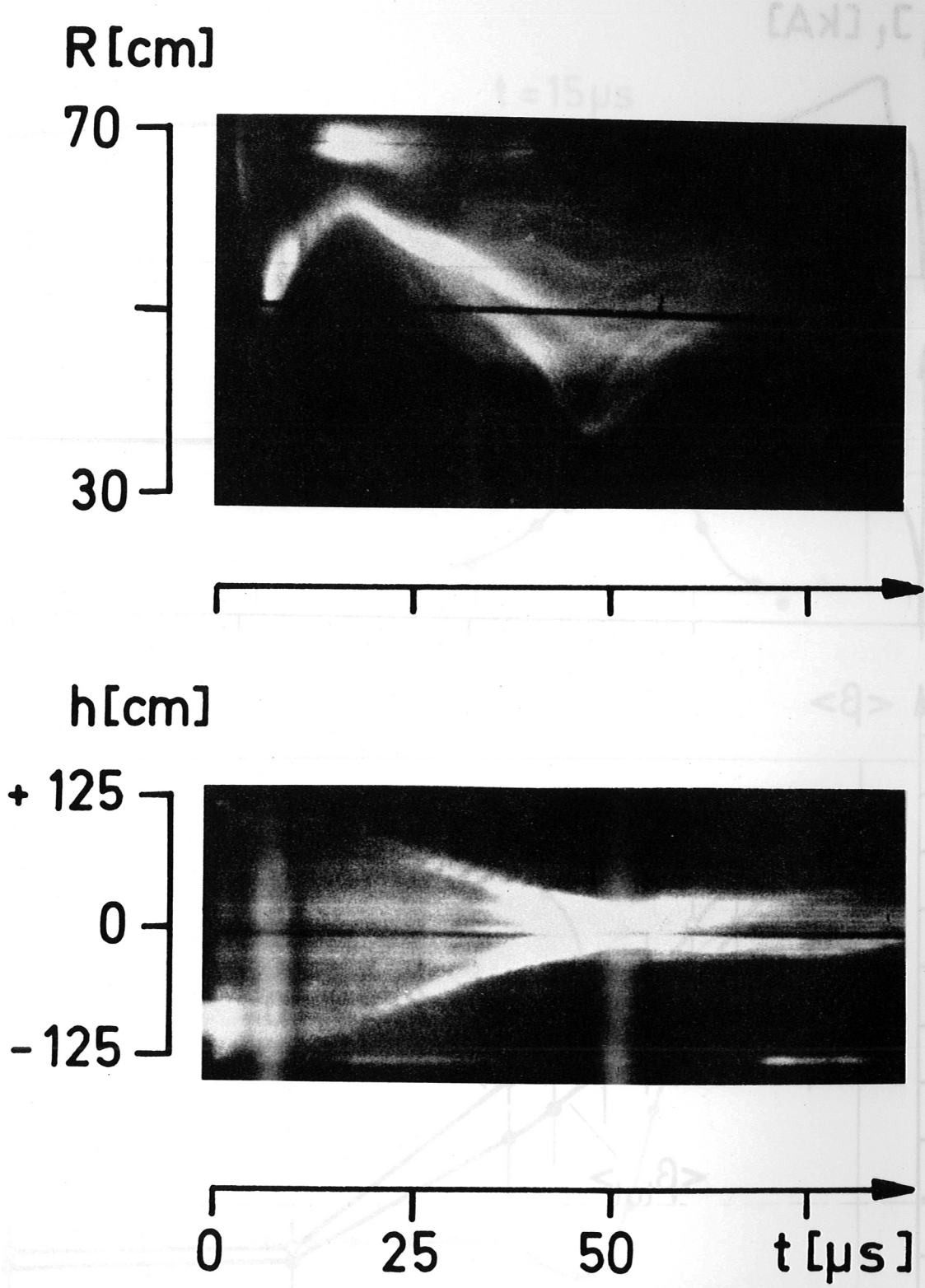


Fig. 9

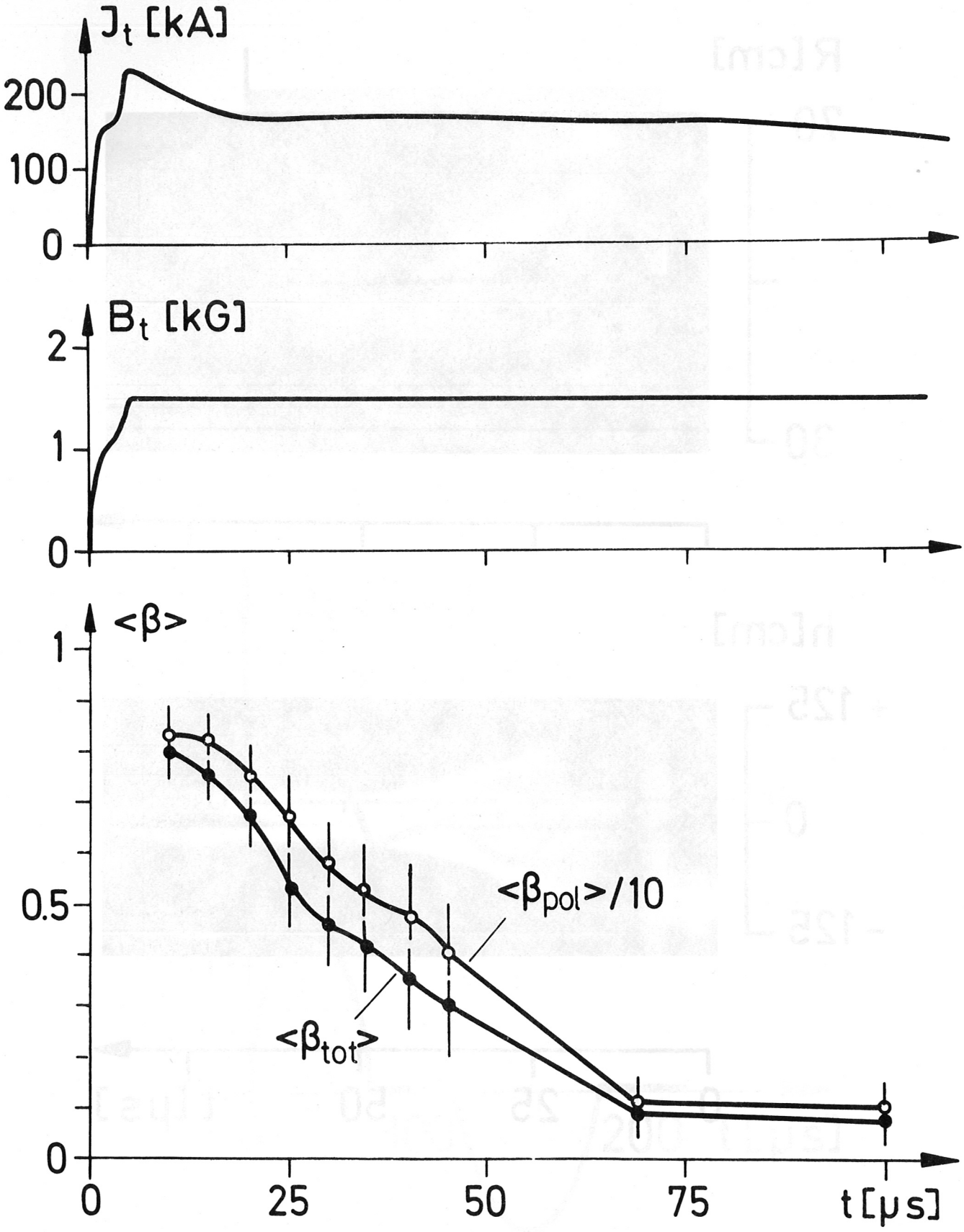


Fig. 10

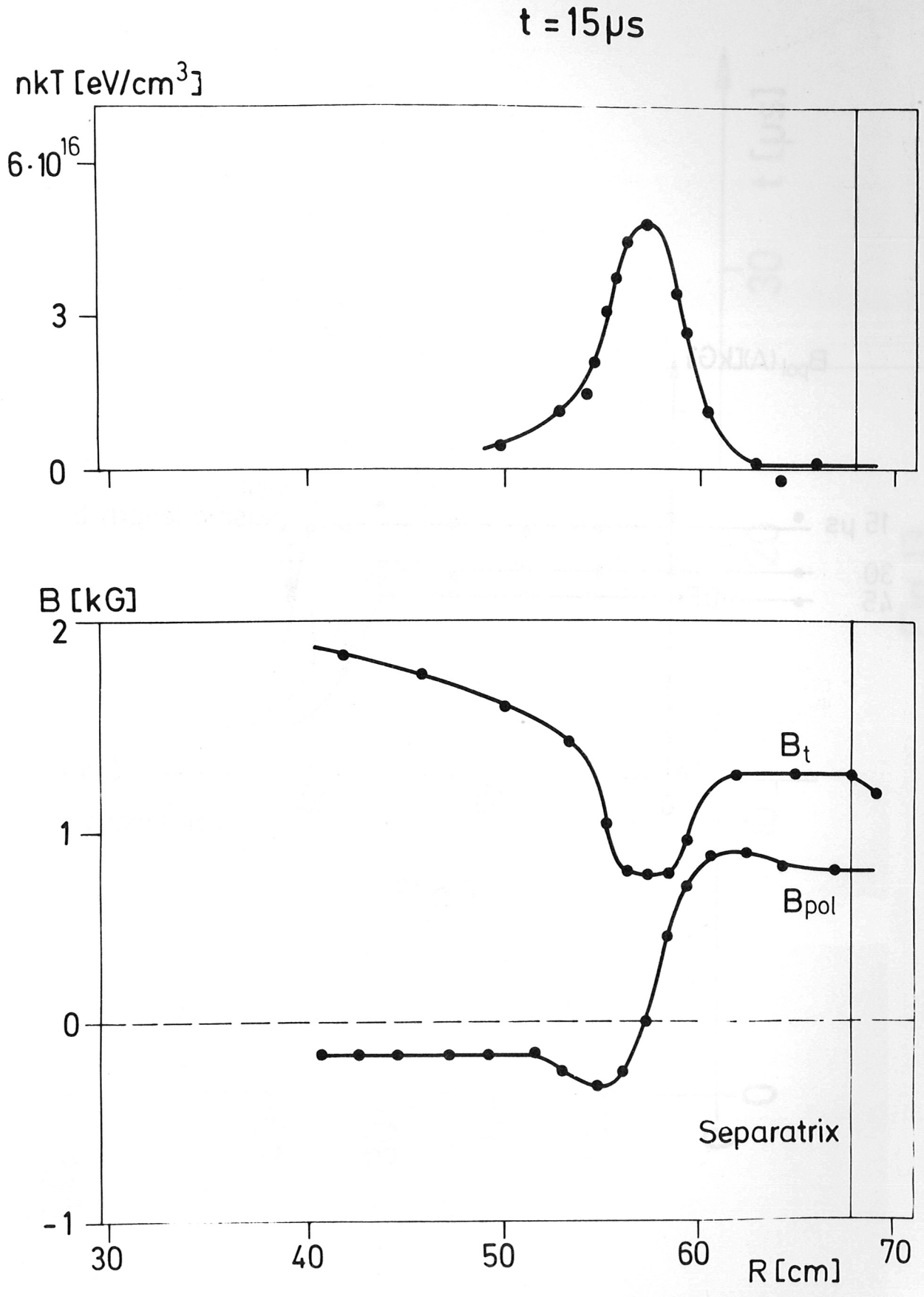
t = 15 μs
nkT [eV/cm³]
6·10¹⁶
3
0
B [kG]
2
1
0
-1
Bt
Bpol
Separatrix
30
40
50
60
70
R [cm]

Fig. 11

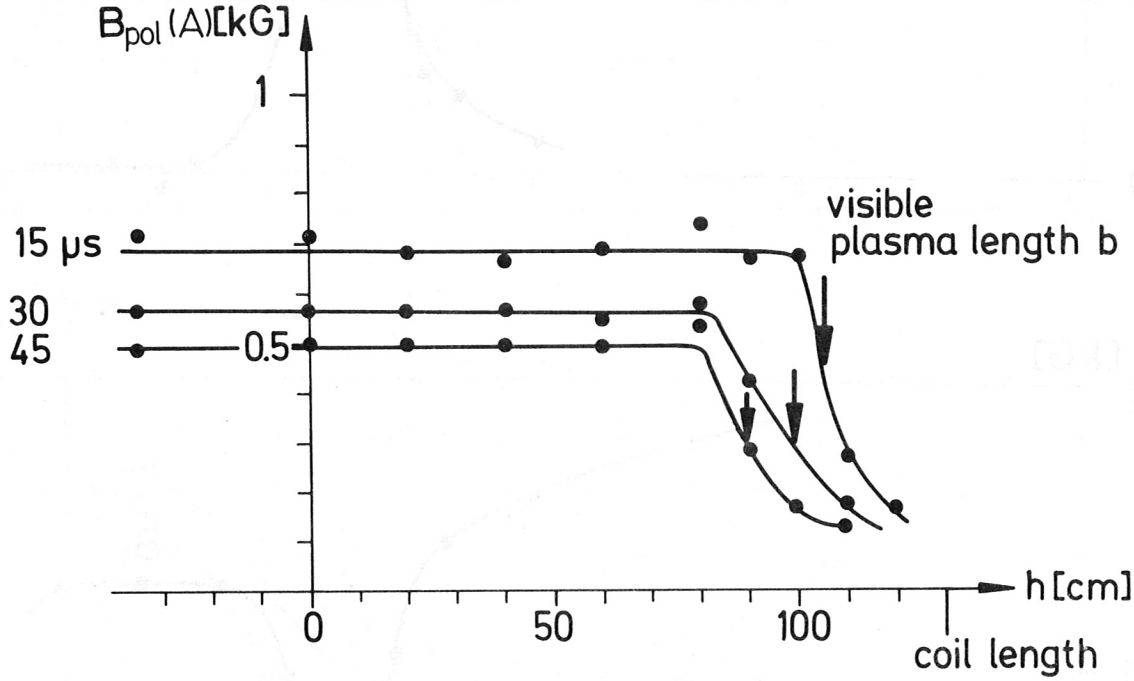
$B_{pol}$ (A)[kG]
1
15 μs
30
45
0.5
visible
plasma length b
h[cm]
0
50
100
coil length

Fig.12

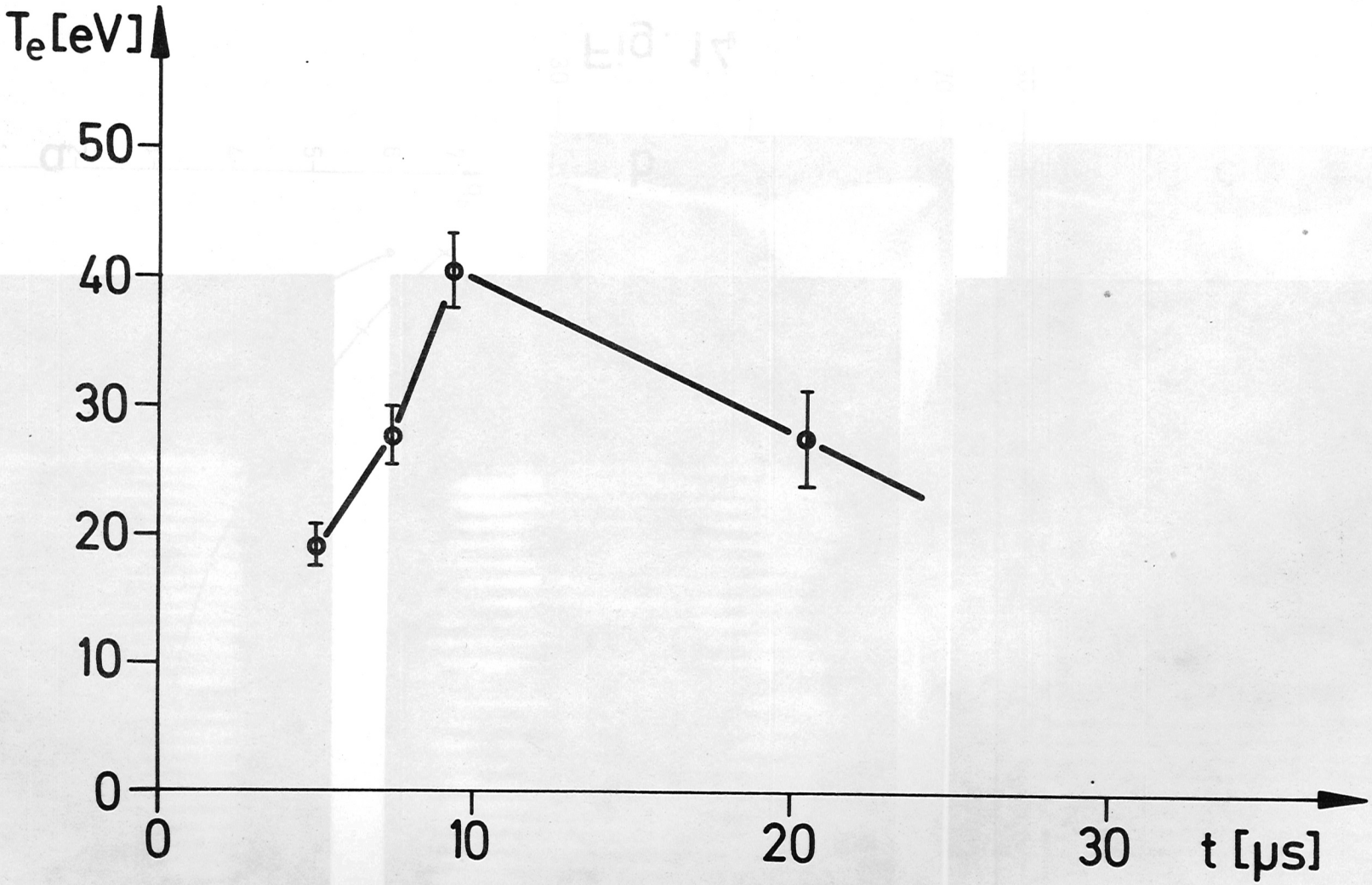


Fig. 13

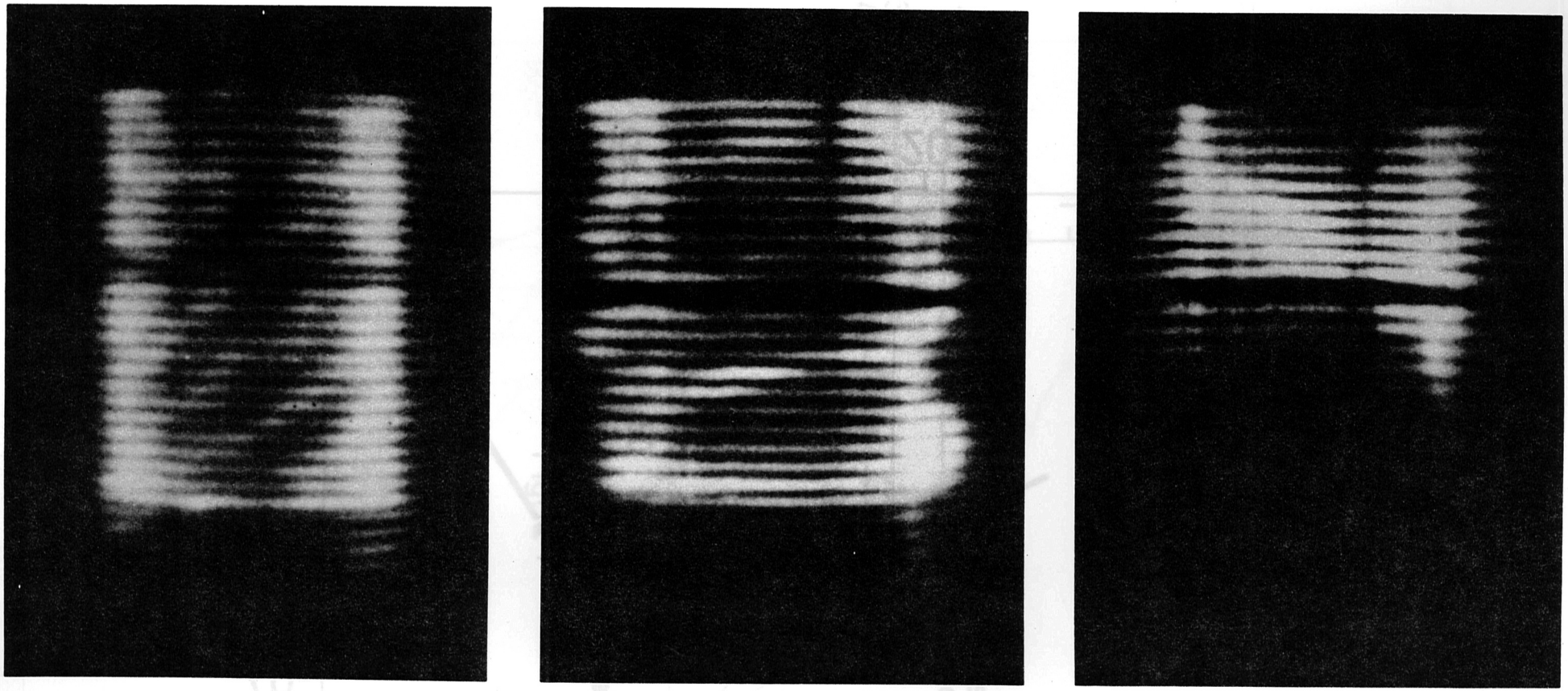

a b c

Fig. 14

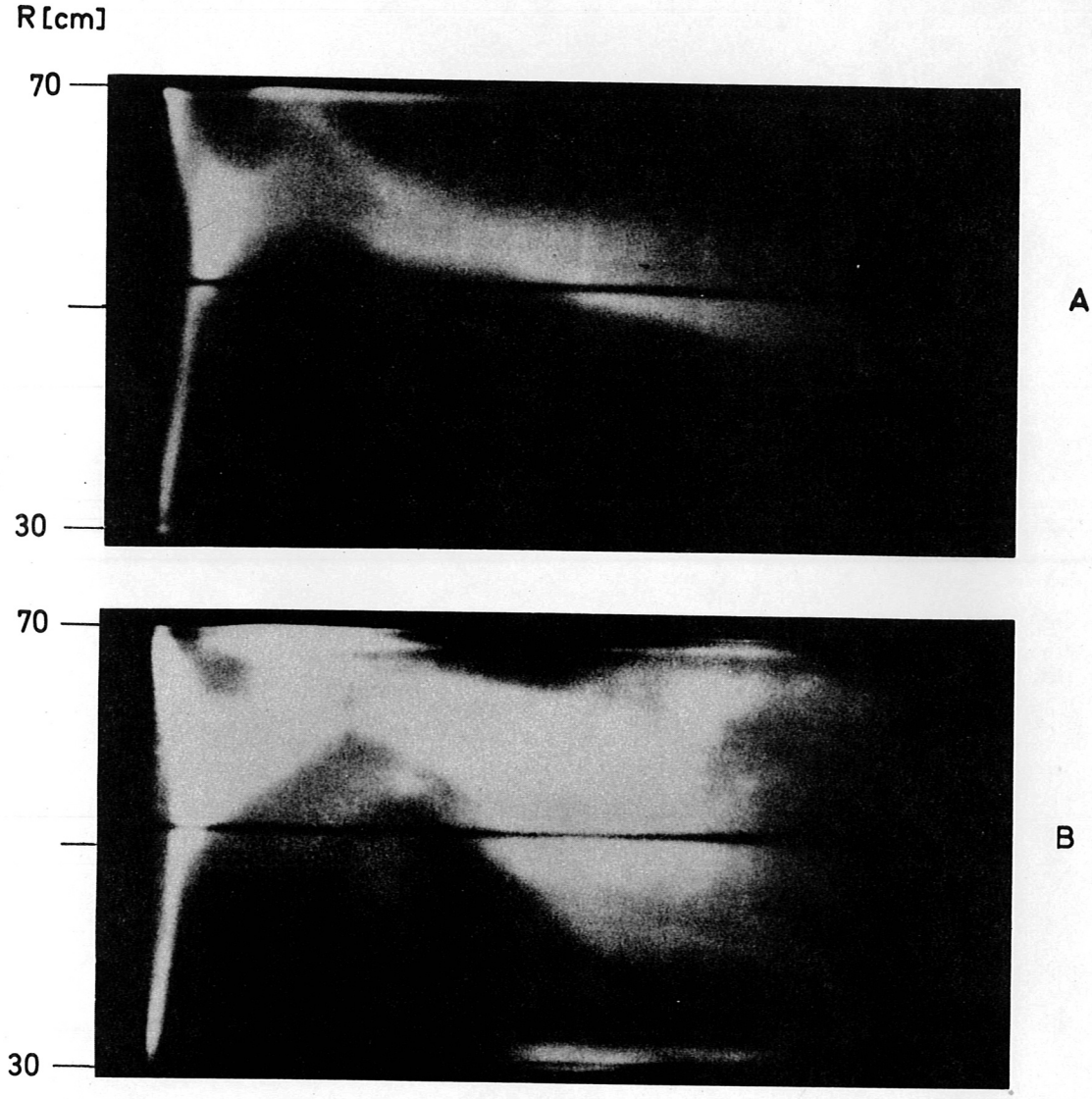
R [cm]
70
30
A
70
30
B

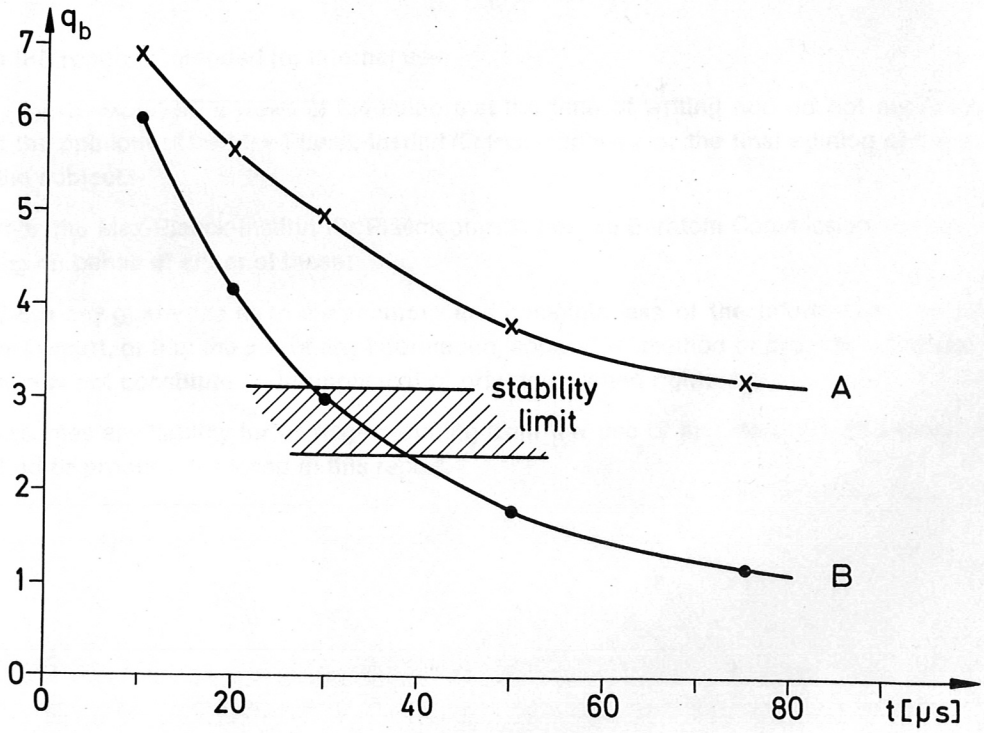
$q_b$
7
6
5
4
3
2
1
0
0
20
40
60
80
t [μs]
stability
limit
A
B

Fig. 15